NANO LETTERS

Letter

pubs.acs.org/NanoLett

Highly Efficient Retention of Polysulfides in "Sea Urchin"-Like Carbon Nanotube/Nanopolyhedra Superstructures as Cathode Material for Ultralong-Life Lithium−Sulfur Batteries

Tao Chen,[†] Baorui Cheng,[†] Guoyin Zhu,[†] Renpeng Chen,[†] Yi Hu,[†] Lianbo Ma,[†] Hongling Lv,[†] Yanrong Wang,[†] Jia Liang,[†] Zuoxiu Tie,[‡] Zhong Jin,*[,†] and Jie Liu*[,†,§]

[†]Key Laboratory of Mesoscopic Chemistry of MOE and Collaborative Innovation Center of Chemistry for Life Sciences, School of Chemistry and Chemical Engineering, Nanjing University, Nanjing, Jiangsu 210023, China

[‡]Department of Engineering and Applied Sciences, Nanjing University, Nanjing, Jiangsu 210023, China

[§]Department of Chemistry, Duke University, Durham, North Carolina 27708, United States

Supporting Information

ABSTRACT: Despite high theoretical energy density, the practical deployment of lithium−sulfur (Li−S) batteries is still not implemented because of the severe capacity decay caused by polysulfide shuttling and the poor rate capability induced by low electrical conductivity of sulfur. Herein, we report a novel sulfur host material based on "sea urchin"-like cobalt nanoparticle embedded and nitrogen-doped carbon nanotube/nanopolyhedra (Co-NCNT/NP) superstructures for Li−S batteries. The hierarchical micromesopores in Co-NCNT/NP can allow efficient impregnation of sulfur and block diffusion of soluble polysulfides by physical confinement, and the incorporation of embedded Co nanoparticles and nitrogen doping (~4.6 at. %) can synergistically improve the adsorption of polysulfides, as evidenced by beaker cell tests. Moreover, the conductive networks of Co-NCNT/NP interconnected by nitrogen-doped carbon nanotubes (NCNTs) can facilitate electron transport and electrolyte infiltration. Therefore, the specific capacity, rate capability, and cycle stability of Li−S batteries are significantly enhanced. As a result, the Co-NCNT/NP based cathode (loaded with 80 wt % sulfur) delivers a high discharge capacity of 1240 mAh g^{-1} after 100 cycles at 0.1 C (based on the weight of sulfur), high rate capacity (755 mAh g^{-1} at 2.0 C), and ultralong cycling life (a very low capacity decay of 0.026% per cycle over 1500 cycles at 1.0 C). Remarkably, the composite cathode with high areal sulfur loading of 3.2 mg cm^{-2} shows high rate capacities and stable cycling performance over 200 cycles.

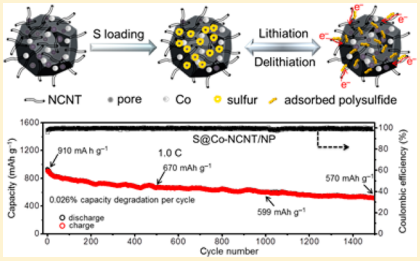

KEYWORDS: *Lithium−sulfur batteries, polysulfide trapping, hierarchical micromesopores, carbon nanotube/nanopolyhedra superstructures*

Lithium−sulfur (Li−S) batteries have attracted intense attention as promising next-generation secondary batteries due to the high theoretical capacity (~1672 mAh g^{-1}) and energy density (~2600 Wh kg^{-1}) of sulfur cathodes.[1−3] However, several major obstacles still limit the practical application of Li−S batteries, including: (1) the huge volume expansion of sulfur upon lithiation, (2) the diffusion of intermediate lithium polysulfides in the electrolyte, and (3) the low electrical conductivity of sulfur and lithium sulfide (Li_2S).[4−6] As a consequence, Li−S batteries usually suffer from fast capacity fading, low Coulombic efficiency, and poor cyclic performance.

As discussed in a recent review,[7] to address the above problems, various strategies, including the development of cathode materials,[8−10] electrolytes,[11,12] and protected anodes,[13] have been proposed to enhance the overall performance of Li−S batteries. A promising approach is to design composite cathodes with porous carbon matrix, such as micro/mesoporous carbons,[14] porous hollow carbon nanospheres,[15,16] carbon nanofibers/nanotubes,[17−19] and graphene.[20] Porous carbon with high surface area can provide large pore volume for encapsulating sulfur and improve the electrical conductivity of sulfur cathode.[21,22] However, the weak interaction between conventional porous carbon and lithium polysulfides is not sufficient to suppress the dissolution of lithium polysulfides in electrolyte.[23] Moreover, an unresolved problem is that the interfacial conductivity and connectivity between the individual pieces of porous carbon is usually low. Therefore, it is important to design novel carbon/sulfur cathodes with high sulfur utilization, less "shuttle effect", and high interfacial conductivity to improve the specific capacity, cycling life and rate capability of Li−S batteries.

Considering that the performances of sulfur host materials are mainly determined by the architecture and compositions, we propose that an ideal carbon/sulfur cathode material should

Received: October 23, 2016
Revised: November 29, 2016
Published: December 5, 2016

DOI: 10.1021/acs.nanolett.6b04433
Nano Lett. 2017, 17, 437−444

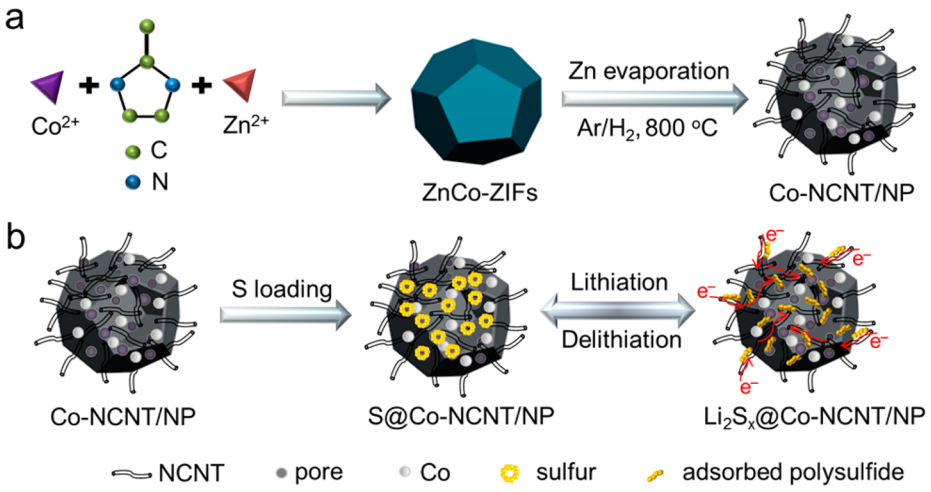

Figure 1. (a) Synthesis process of the Co-NCNT/NP superstructures. (b) Schematic illustration of the trapping mechanism of sulfur and polysulfide species in Co-NCNT/NP superstructures.

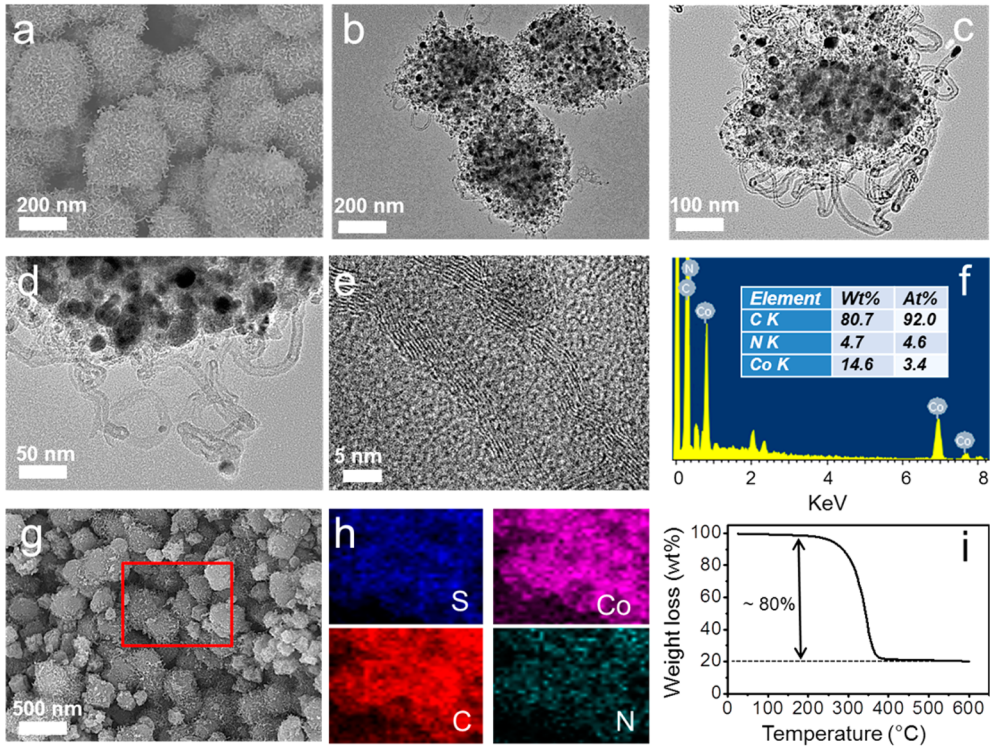

Figure 2. (a) SEM and (b–d) TEM images of "sea urchin"-like Co-NCNT/NP superstructures. (e) High-resolution TEM image of Co-NCNT/NP, revealing the multiwalled structure of NCNTs grown on the surface of Co-NCNT/NP. (f) EDX spectrum of Co-NCNT/NP superstructures. (g) SEM image of S@Co-NCNT/NP composite and (h) corresponding EDX elemental mapping of S, Co, C, and N elements collected from the marked area in (g). (i) TGA curve of S@Co-NCNT/NP composite measured in N_2 atmosphere, showing a high sulfur loading ratio of ~80 wt %.

have the following advantageous features: (1) hierarchical porous structure with both abundant interior mesopores with large volume for storing sulfur species, and also surface micropores for the physical confinement of sulfur species;[24,25] (2) doped heteroatoms[26−28] and/or metal nanoparticles[29−31] with strong chemical affinity and strong binding/interactions with sulfur species to promote the adsorption of lithium polysulfides; (3) smooth localized pathways for the transport of Li ions and electrons; (4) high local conductivity, high overall conductivity and interconnected conductive networks for improving sulfur utilization and decreasing inner resistance. Following this line of thought, there are many anticipated benefits to developing novel carbon based superstructures with all of the above-mentioned merits for Li−S batteries.

It is a great challenge to synthesize an ideal structure that satisfies all the requirements discussed above, especially for an economical and scalable process. Interestingly, we developed a scalable process that can prepare "sea urchin"-like Co nanoparticle embedded and nitrogen doped carbon nanotube/nanopolyhedra (Co-NCNT/NP) superstructures that almost ideally suitable for a host material of the sulfur cathode. The Co-NCNT/NP were synthesized by a simple reductive pyrolysis process of Zn and Co bimetallic zeolitic imidazolate frameworks (ZnCo-ZIFs). During the pyrolysis, the evapo-

DOI: 10.1021/acs.nanolett.6b04433
Nano Lett. 2017, 17, 437−444

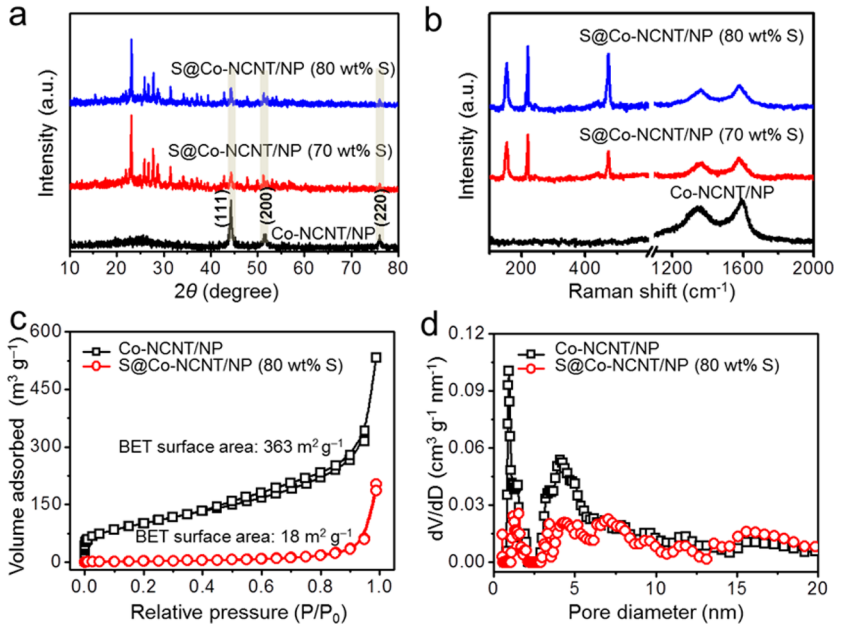

Figure 3. (a) XRD and (b) Raman spectra of pristine Co-NCNT/NP and S@Co-NCNT/NP composites with different sulfur loading ratios. (c) Nitrogen adsorption−desorption isotherms and (d) pore-size distribution of pristine Co-NCNT/NP and S@Co-NCNT/NP composite (with 80 wt % of S).

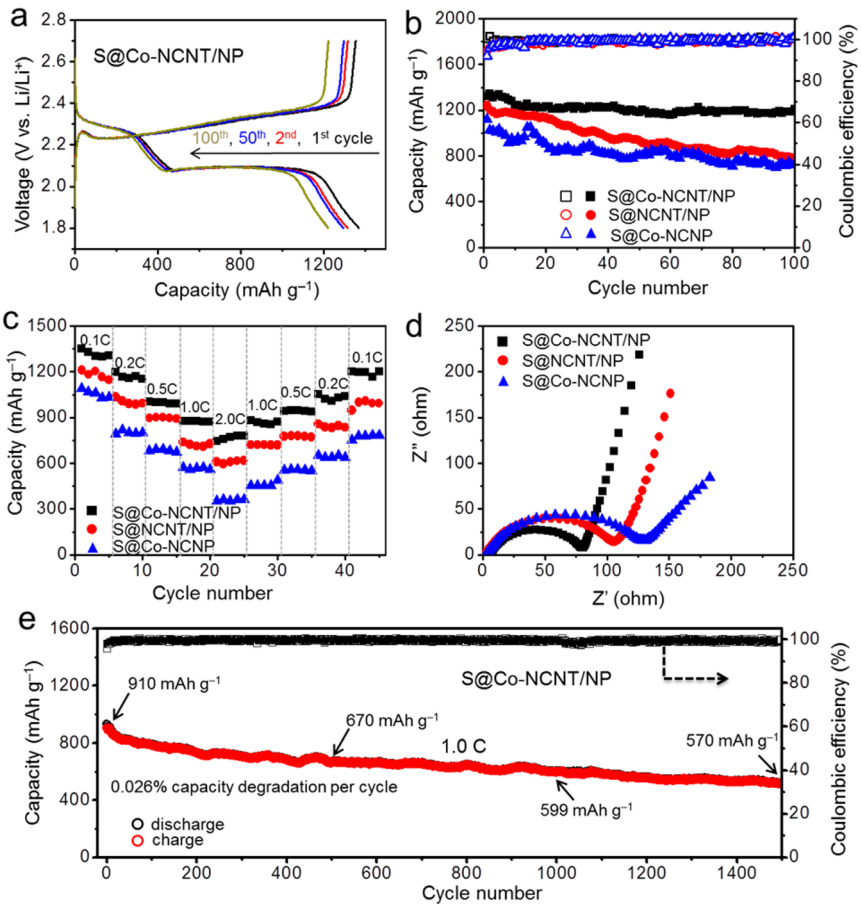

Figure 4. (a) Galvanostatic charge/discharge curves of S@Co-NCNT/NP cathode at 0.1 C in the voltage range of 1.8−2.7 V vs Li^+/Li. (b) Cycling performances and Coulombic efficiencies of S@Co-NCNT/NP, S@NCNT/NP, and S@Co-NCNP electrodes tested at 0.1 C. (c) Rate capabilities and (d) Nyquist plots of the above three sulfur composite cathodes, respectively. (e) Long-term cycling stability of S@Co-NCNT/NP electrode at 1.0 C over 1500 cycles.

DOI: 10.1021/acs.nanolett.6b04433
Nano Lett. 2017, 17, 437−444

ration of Zn leads to the formation of hierarchical micro-mesoporous structures in the Co-NCNT/NP that can facilitate ion and electron transport and restrict polysulfide intermediates diffusion during charge/discharge process. Furthermore, the remaining encapsulated Co nanoparticles and high doping content of nitrogen species in the Co-NCNT/NP not only can strongly immobilize lithium polysulfides through interactions but also can promote redox reactions of polysulfides and inhibit irreversible reactions with carbonate electrolytes.[29,30] In additional, during the reductive pyrolysis process and evaporation process of Zn, large amount of nitrogen-doped carbon nanotubes (NCNTs) were grown on the external surface of Co-NCNT/NP by the catalysis of Co nanoparticles. The interconnected conductive network formed by out-stretched NCNTs can provide an open structure to improve electrolyte infiltration and electron transportation throughout the entire electrode. With the synergistic effect of embedded Co nanoparticles, nitrogen doping, hierarchical micromeso-pores, and interconnected NCNTs, the Co-NCNT/NP based sulfur cathode with a high sulfur loading of 80 wt % shows a high initial capacity of 1350 mAh g^{-1} at 0.1 C based on the weight of sulfur, and cycling stability of only 0.026% capacity decay per cycle over 1500 cycles at 1.0 C. More importantly, the Co-NCNT/NP based sulfur cathode with a high areal sulfur loading of 3.2 mg cm^{-2} showed high rate capacities and stable cycling performance over 200 cycles. These performances show that the material is among the best host materials reported in the literature as summarized in a recent review article.[7]

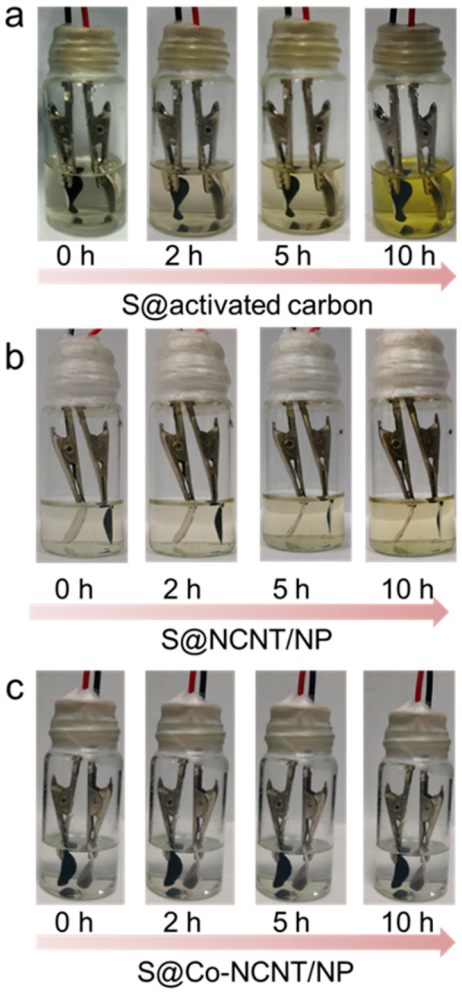

Figure 5. Beaker cell tests of Li–S batteries for the visual comparison of polysulfide entrapment. (a) S@activated carbon, (b) S@NCNT/NP, and (c) S@Co-NCNT/NP composite cathodes with the same sulfur loading ratio of 80 wt % recorded at different time during the first discharge process at 0.1 C.

For the preparation of Co-NCNT/NP, bimetallic ZnCo-ZIFs containing Zn^{2+}, Co^{2+}, and 2-methylimidazolate were chosen as precursor materials. Uniform polyhedral ZnCo-ZIFs with average diameters of 300–400 nm (Figure S1) were synthesized according to a reported method with minor modification.[32] As illustrated in Figure 1a, the Co-NCNT/NP superstructures were synthesized by direct pyrolysis of as-prepared ZnCo-ZIFs at 800 °C for 3 h in a reductive Ar/H_2 atmosphere. With the volatilization of Zn metal and the formation of porous structure, the nanopolyhedra of ZnCo-ZIFs were converted to N-doped porous carbon scaffolds with embedded Co nanoparticles during the pyrolysis process. Subsequently, the encapsulated Co nanoparticles catalyzed the growth of a large number of NCNTs on the surface of carbon scaffolds under the reductive atmosphere.

Sulfur was impregnated into the as-synthesized Co-NCNT/NP superstructures by a typical melt-diffusion method.[33] The trapping mechanism of sulfur and polysulfides in Co-NCNT/NP superstructures is illustrated in Figure 1b. During the discharge processes, the hierarchical micromesopore structure of Co-NCNT/NP can inhibit the dissolution and leakage of soluble lithium polysulfides by physical entrapment. Additionally, the nitrogen-heteroatoms and Co nanoparticles can strongly bind with adsorbed polysulfides to alleviate the polysulfides shuttling, and also greatly enhance the redox reaction kinetics of polysulfides. Finally, the interconnected NCNTs grown on the surface of "sea urchin"-like Co-NCNT/NP can enhance the local and overall electrical conductivity of electrode, improve the sulfur utilization, and increase the structural stability of the entire electrode. As the last line of defense, the interconnected NCNTs can further prevent outward diffusion of polysulfides, achieving the long-term cycling process.

Figure 2a shows a typical scanning electron microscopy (SEM) image of as-prepared Co-NCNT/NP superstructures. It is observed that the morphology of Co-NCNT/NP seems to change from the regular polyhedra of the precursor to relatively irregular shape, arising from a large number of intertwined carbon nanotubes anchored on the rough surface of carbon nanopolyhedra. Transmission electron microscopy (TEM) images (Figure 2b–d) of Co-NCNT/NP confirmed that plenty of NCNTs with the length of 100–300 nm and diameter of around 10–15 nm are grown on the outboard of carbon nanopolyhedra. Size statistics and high-resolution TEM image (Figure S2) revealed that crystalline Co nanoparticles with the diameter between 8–26 nm are homogeneously embedded in Co-NCNT/NP and possess lattice fringes of 0.20 nm, consistent with the face-centered cubic Co(111) planes. The graphitic layers of the multiwalled NCNTs grown on the surface of Co-NCNT/NP are not completely parallel (Figure 2e), indicating the existence of abundant defect sites.[34] Energy-dispersive X-ray spectroscopy (EDX) clearly confirmed the presence of C, Co, and N elements in Co-NCNT/NP superstructures (Figure 2f).

As two control samples, N-doped carbon nanotube/nanopolyhedra without embedded Co nanoparticles (NCNT/NP) and Co-embedded N-doped carbon nanopolyhedra without

DOI: 10.1021/acs.nanolett.6b04433
Nano Lett. 2017, 17, 437–444

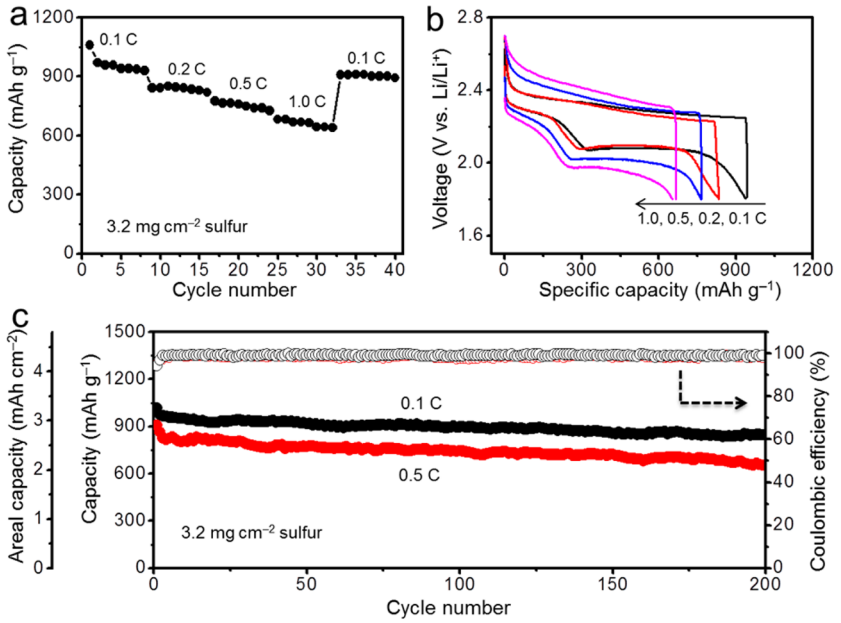

Figure 6. (a) Rate performance and (b) voltage profiles of S@Co-NCNT/NP with a sulfur loading of 3.2 mg cm^{-2} at different current rates. (c) Cycling performance of S@Co-NCNT/NP at 0.1 and 0.5 C over 200 cycles.

exterior NCNTs (Co-NCNP) were also synthesized (Figure S3a,b), as detailed in the experimental section. After the encapsulation of elemental sulfur via a melt-diffusion method, the composite cathode materials based on Co-NCNT/NP, NCNT/NP, and Co-NCNP are termed as S@Co-NCNT/NP, S@NCNT/NP, and S@Co-NCNP, respectively. To identify the components of S@Co-NCNT/NP composite, elemental mapping was carried out with energy-dispersive X-ray spectrometer (EDX) attached to the SEM instrument. SEM image (Figure 2g) and corresponding EDX elemental mapping (Figure 2h) of S@Co-NCNT/NP composite clearly confirmed the existence of evenly dispersed S, C, Co, and N elements. No bulky aggregation or small particles of sulfur were found at the outer surface of S@Co-NCNT/NP, suggesting the thorough encapsulation and homogeneous distribution of S inside S@Co-NCNT/NP. The content of sulfur in S@Co-NCNT/NP composite was measured by thermogravimetric analysis (TGA), showing a high loading ratio of ~80 wt % (Figure 2i).

The crystallinity of pristine Co-NCNT/NP and S@Co-NCNT/NP composites with different sulfur contents are verified by powder X-ray diffraction (XRD) as shown in Figure 3a. The XRD spectrum of pristine Co-NCNT/NP shows two diffraction peaks around 44.2°, 51.6°, and 75.9°, corresponding to the (111), (200), and (220) lattice planes of Co nanoparticles (JCPDS no. 89-4307).[29] The XRD spectra of S@Co-NCNT/NP composites also proves the presence of sulfur and Co. Raman spectroscopy was performed to investigate the structural features of carbon and sulfur in Co-NCNT/NP and S@Co-NCNT/NP composites (Figure 3b). Two prominent characteristic peaks of carbon at 1346 cm^{-1} (D band) and 1595 cm^{-1} (G band) are attributed to disordered/defective carbon and graphitic carbon, respectively. With the increase of sulfur content in the S@Co-NCNT/NP composites, the intensities of D and G bands became weaker, while three peaks of elemental sulfur at 470, 217, and 150 cm^{-1} became stronger, confirming the confinement of sulfur in the S@Co-NCNT/NP. Nitrogen adsorption/desorption isotherms of Co-NCNT/NP show the joint of type I and IV isotherms (Figure 3c), indicating the presence of both micropores and mesopores. The pore size distribution of Co-NCNT/NP was analyzed by nonlocal density functional theory (NLDFT) method, revealing the existence of mesopores with size centered at 4.0 nm and abundant micropores with an average size of 0.9 nm (Figure 3d). Brunauer–Emmett–Teller (BET) surface area of Co-NCNT/NP was calculated to be 363 m^2 g^{-1}. In contrast, the specific surface area of S@Co-NCNT/NP with a sulfur loading ratio of 80 wt % remarkably decreased to 18 m^2 g^{-1} and the pore volume also significantly reduced from 0.67 m^3 g^{-1} to 2.3 × 10^{-7} m^3 g^{-1}, confirming the full encapsulation of sulfur in the pores.

To confirm the interactions between sulfur and Co-NCNT/NP, X-ray photoelectron spectroscopy (XPS) was conducted (Figures S4 and S5). The high-resolution XPS spectrum of S@Co-NCNT/NP composite at C 1s region reveals two bands at 284.5 and 285.6 eV, contributed by C═C and C═N bonds, respectively (Figure S5a). Two peaks at S 2p region around 163.6 and 164.8 eV can be assigned to S 2p$_{3/2}$ and S 2p$_{1/2}$, confirming the existence of S_8 molecules in mesopores. Another weak peak located at 168.7 eV is ascribed to a small amount of sulfate species formed by the oxidation of sulfur in air (Figure S5b).[35] The S content of S@Co-NCNT/NP composite measured by XPS is only 15.3 wt %, much lower than that calculated by TGA analysis (Figure 2i). This result suggests that part of sulfur is deposited on the surfaces of Co-NCNT/NP. The Co 2p$_{3/2}$ spectrum exhibits two peaks at 778.5 and 780.3 eV (Figure S5c), corresponding to metallic cobalt and N-coordinated Co^{2+} (Co–N$_x$), respectively.[36] The N 1s band of S@Co-NCNT/NP can be deconvoluted into three characteristic peaks: pyridinic, pyrrolic, and graphitic N species located at 398.6, 400.8, and 401.3 eV, respectively (Figure S5d). The nitrogen heteroatoms are favorable for the wettability and binding of sulfur species within carbon matrix,[37,38] thus beneficial to improve the cycle stability and rate capability of Li–S batteries.

The electrochemical performances of S@Co-NCNT/NP composite (with 80 wt % of S) were evaluated as cathode

DOI: 10.1021/acs.nanolett.6b04433
Nano Lett. 2017, 17, 437–444

material for Li−S batteries with an average sulfur mass loading of 1.2 mg cm^{-2}. Cyclic voltammetric (CV) curves of S@Co-NCNT/NP cathode at a sweep rate of 0.1 mV s^{-1} are shown in Figure S6a. In the first cathodic scan, two well-defined peaks were observed at 2.28 and 2.05 V, respectively. The reduction peak at 2.28 V is associated with the reduction of element sulfur to lithium polysulfides (Li_2S_n, $4 < n < 8$), while another reduction peak at 2.05 V corresponds to the further reduction of lithium polysulfides to insoluble Li_2S_2 and solid Li_2S.[38,39] In the subsequent anodic scan, there is a broad peak at ∼2.32 V associated with the reverse conversion from lithium polysulfides to element sulfur during the charging process. From the second cycle, the CV curves of S@Co-NCNT/NP remain almost overlapped, indicating effective suppression of the electrochemical polarization by Co-NCNT/NP. Notably, when compared to the CV profile of S@NCNT/NP cathode (Figure S6b), the S@Co-NCNT/NP and S@Co-NCNP composites incorporated with embedded Co nanoparticles exhibit faster electrochemical reaction kinetics, which is evidenced by the increase of cathodic peak and the decrease of anodic peak for 25−30 mV, respectively.

The representative galvanostatic charge/discharge profiles of S@Co-NCNT/NP cathode between 1.8 and 2.7 V at 0.1 C (1 C = 1675 mAh g^{-1}) are shown in Figure 4a. The S@Co-NCNT/NP cathode exhibits two discharging plateaus and one charging plateau at 0.1 C, which is consistent with the CV curves. Overall, the charge/discharge profiles of S@NCNT/NP and S@Co-NCNP cathodes during the first discharge cycle are similar to that of S@Co-NCNT/NP but with relatively lower energy capacities (Figure S7). The cycling performances of S@Co-NCNT/NP, S@NCNT/NP, and S@Co-NCNP cathodes at 0.1 C were depicted in Figure 4b. The S@Co-NCNT/NP cathode can deliver a remarkable initial reversible capacity as high as 1350 mAh g^{-1} and still retain a stable capacity of 1240 mAh g^{-1} after 100 cycles, corresponding to a capacity retention of 92%. In contrast, the S@NCNT/NP and S@Co-NCNP cathodes have initial reversible capacities of 1240 and 1120 mAh g^{-1} and preserve the discharge capacities of 786 and 720 mAh g^{-1} after 100 cycles, respectively.

For further comparison, the rate performances of all the samples were evaluated at various current rates. The typical galvanostatic charge/discharge profiles of S@Co-NCNT/NP cathode at different current densities of 0.1, 0.2, 0.5, 1.0, and 2.0 C are depicted in Figure S8. The discharge profiles exhibit typical two-plateau behavior, corresponding to the formation of polysulfides (Li_2S_n, $4 < n < 8$) at 2.32 V and short-chain Li_2S_2 and Li_2S at 2.1 V. Although the potential of discharge plateau slightly decreases at high current rate of 2.0 C, the platforms are still clear. At a low current density of 0.1 C, a discharge capacity of 1310 mAh g^{-1} was obtained from S@Co-NCNT/NP cathode at the fifth cycle (Figure 4c). When the current rates were increased to 0.2, 0.5, 1.0, and 2.0 C, the electrode exhibits reversible capacities of 1190, 1000, 875, and 775 mAh g^{-1}, respectively. Compared with the S@NCNT/NP and S@Co-NCNP cathodes, the S@Co-NCNT/NP cathode exhibited much higher capacity at the same discharge rates (Figure 4c). As the current rate decreased back to 0.1 C, the specific capacity of S@Co-NCNT/NP cathode recovered to 1195 mAh g^{-1}, indicating good stability and structural integrity of the electrode.

For comparing the internal resistances of the three composite cathodes, electrochemical impedance spectroscopy (EIS) was performed (Figure 4d). As presented by the high-frequency semicircles in the Nyquist plots, the charge-transfer resistance (R_{ct}) of S@Co-NCNT/NP is lower than those of S@NCNT/NP and S@Co-NCNP, indicating the Co-NCNT/NP superstructures offer faster ion diffusion and higher electrical conductivity.

To evaluate the long-term cycling stability, the Li−S batteries based on S@Co-NCNT/NP cathodes were cycled at high current densities (Figure 4e). At the current rate of 1.0 C, the S@Co-NCNT/NP cathode delivers initial discharge and charge capacities of 930 and 908 mAh g^{-1}, respectively. After 500 cycles, the specific capacity of S@Co-NCNT/NP is well maintained at 670 mAh g^{-1}, with a capacity retention of 72% and Coulombic efficiency of 99.7%. The discharge capacity remains as high as 570 mAh g^{-1} even after 1500 cycles, which corresponds to a low capacity decay of only 0.026% per cycle. As the current rate increased to 2.0 C, the S@Co-NCNT/NP cathode exhibits a reversible capacity of 795 mAh g^{-1} and maintains at 495 mAh g^{-1} after 800 cycles, with a low capacity fade rate of 0.047% per cycle (Figure S9). Moreover, TEM observation indicates that the overall morphology and structural integrity of S@Co-NCNT/NP composite cathode was still preserved after 800 cycles at 2.0 C (Figure S10). After the long-term cycling test, sulfur and intermediate polysulfides were still effectively confined within the composite cathode (Figure S11a), as confirmed by the little change in sulfur content of the S@Co-NCNT/NP composite (Figure S11c). Almost no aggregated large sulfur particles were observed outside the cycled S@Co-NCNT/NP electrode (Figure S11b), owing to the synergetic effect of physical confinement and chemical affinity. Compared with the pristine S@Co-NCNT/N composite, the "sea urchin"-like nanostructures were well preserved after cycling. Considering the low capacity decay rate and ultralong cycle life, the electrochemical performance of S@Co-NCNT/NP composite is among the best host materials reported in the literature.[7,17,20,24,28,29,40]

To understand the superb capability of Co-NCNT/NP for trapping soluble polysulfides, beaker cell tests were carried out. The color changes of the electrolyte in the sealed beaker cells with sulfur composite cathode and lithium foil anode were recorded at different time of the discharge process. As a control sample, a sulfur composite cathode was prepared by filling sulfur into commercially available activated carbon (S@activated carbon) via the same melt-diffusion process. The electrolyte in the cell based on S@activated carbon cathode quickly turned into yellow color (Figure 5a), indicating the dissolution and leakage of lithium polysulfides into the electrolyte. For the S@NCNT/NP composite, the color of electrolyte gradually changed from colorless to canary yellow after the discharge process, suggesting a small fraction of intermediate polysulfides were dissolved in the electrolyte. In contrast, the electrolyte in the cell based on S@Co-NCNT/NP cathode remain colorless throughout the first discharge process (Figure 5b), which demonstrates the remarkable polysulfide trapping capability of S@Co-NCNT/NP cathode in Li−S batteries.

Considering the high areal capacity is critical for practical application of Li−S batteries, the areal sulfur loading was increased to approximately 3.2 mg cm^{-2} by fabricating a thick-film electrode. The rate capability of the S@Co-NCNT/NP cathode with high areal sulfur loading of 3.2 mg cm^{-2} was assessed at various current densities from 0.1 to 1 C (Figure 6a,b). The cathode shows discharge capacities of 960, 845, 760, and 668 mAh g^{-1} at 0.1, 0.2, 0.5, and 1.0 C, respectively, which

DOI: 10.1021/acs.nanolett.6b04433
Nano Lett. 2017, 17, 437−444

correspond to areal capacities of 3.1, 2.7, 2.4, and 2.1 mAh cm^{-2}. When the current rate is back to 0.1 C, the S@Co-NCNT/NP cathode delivers a reversible capacity of 899 mAh g^{-1} (2.9 mAh cm^{-2}), suggesting high stability of electrode structure. The cycling performance of S@Co-NCNT/NP is shown in Figure 6c. The S@Co-NCNT/NP composite exhibits an initial capacity of 1017 mAh g^{-1} (3.2 mAh cm^{-2}) at 0.1 C and still maintains a stable discharge capacity of 846 mAh g^{-1} (2.7 mAh cm^{-2}) at the 200th cycle. When cycled at 0.5 C, the discharge capacity slowly decreased from 908 to 657 mAh g^{-1} (2.1 mAh cm^{-2}) by the 200 cycle. The excellent electrochemical performances of S@Co-NCNT/NP cathode can be attributed to the special compositions and structures. First, the hierarchical micromesopores are effective for the encapsulation and physical confinement of a large loading ratio of sulfur. Second, the embedded Co nanoparticles and nitrogen doping provide strong interaction with adsorbed polysulfides and also greatly enhance the redox reaction kinetics of polysulfides. Third, the interconnected NCNTs on the surface of S@Co-NCNT/NP form a three-dimensional conductive network, which facilitates the local and overall electron transportation during the cycling processes, thus improving the utilization of sulfur.

In conclusion, starting with bimetallic ZnCo-ZIFs as precursor, "sea urchin"-like Co-NCNT/NP superstructures have been synthesized as novel and high performance sulfur host for Li−S batteries. The Li−S batteries based on S@Co-NCNT/NP cathode deliver high reversible specific capacity, good rate capability, and ultralong and excellent cycling stability, owing to the rationally designed nanoarchitecture and components. More importantly, the S@Co-NCNT/NP cathode with a high areal sulfur loading of 3.2 mg cm^{-2} shows high rate capacities and stable cycling performance over 200 cycles. This strategy provides new insights for the construction of advanced sulfur host materials with metal−organic precursors for achieving high-performance Li−S batteries.

■ ASSOCIATED CONTENT

Supporting Information

The Supporting Information is available free of charge on the ACS Publications website at DOI: 10.1021/acs.nanolett.6b04433.

Experimental details, supplementary characterizations including SEM, TEM, XPS, and other electrochemical measurements (PDF)

■ AUTHOR INFORMATION

Corresponding Authors

*(Z.J.) E-mail: zhongjin@nju.edu.cn.
*(J.L.) E-mail: j.liu@duke.edu.

ORCID

Tao Chen: 0000-0003-2536-4145
Zhong Jin: 0000-0001-8860-8579
Jie Liu: 0000-0003-0451-6111

Notes

The authors declare no competing financial interest.

■ ACKNOWLEDGMENTS

This work was supported by National Materials Genome Project (2016YFB0700600), National 973 Basic Research Program (2015CB659300), National Natural Science Foundation of China (21403105, 21573108), China Postdoctoral Science Foundation (2015M581768, 2015M580413), Natural Science Foundation for Young Scholars of Jiangsu Province (BK20150583, BK20160647), Fundamental Research Funds for the Central Universities, and a project funded by the Priority Academic Program Development (PAPD) of Jiangsu Higher Education Institutions.

■ REFERENCES

(1) Yang, Y.; Zheng, G. Y.; Cui, Y. *Chem. Soc. Rev.* **2013**, *42*, 3018−3032.
(2) Zhou, G. M.; Li, L.; Ma, C. Q.; Wang, S. G.; Shi, Y.; Koratkar, N.; Ren, W.; Li, F.; Cheng, H. M. *Nano Energy* **2015**, *11*, 356−365.
(3) Yin, Y. X.; Xin, S.; Guo, Y. G.; Wan, L. J. *Angew. Chem., Int. Ed.* **2013**, *52*, 13186−13200.
(4) Evers, S.; Nazar, L. F. *Acc. Chem. Res.* **2012**, *46*, 1135−1143.
(5) Manthiram, A.; Fu, Y.; Su, Y. S. *Acc. Chem. Res.* **2012**, *46*, 1125−1134.
(6) Manthiram, A.; Fu, Y.; Chung, S. H.; Zu, C.; Su, Y. S. *Chem. Rev.* **2014**, *114*, 11751−11787.
(7) Seh, Z. W.; Sun, Y. M.; Zhang, Q. F.; Cui, Y. *Chem. Soc. Rev.* **2016**, *45*, 5605−5634.
(8) Ji, X.; Lee, K. T.; Nazar, L. F. *Nat. Mater.* **2009**, *8*, 500−506.
(9) Seh, Z. W.; Li, W. Y.; Cha, K. J. J.; Zheng, G. Y.; Yang, Y.; McDowell, M. T.; Hsu, P.-C.; Cui, Y. *Nat. Commun.* **2013**, *4*, 1331.
(10) Xin, S.; Gu, L.; Zhao, N. H.; Yin, Y. X.; Zhou, L. J.; Guo, Y. G.; Wan, L. J. J. *J. Am. Chem. Soc.* **2012**, *134*, 18510−18513.
(11) Lin, Z.; Liu, Z.; Fu, W.; Dudney, N. J.; Liang, C. *Angew. Chem.* **2013**, *125*, 7608−7611.
(12) Lin, Z.; Liu, Z.; Fu, W.; Dudney, N. J.; Liang, C. *Adv. Funct. Mater.* **2013**, *23*, 1064−1069.
(13) Huang, C.; Xiao, J.; Shao, Y. Y.; Zheng, J. M.; Bennett, W. D.; Lu, D. P.; Saraf, L. V.; Engelhard, M.; Ji, L. W.; Zhang, J. G.; Li, X. L.; Graff, G. L.; Liu, J. *Nat. Commun.* **2015**, *5*, 3015.
(14) Li, Z.; Jiang, Y.; Yuan, L. X.; Yi, Z. Q.; Wu, C.; Liu, Y.; Strasser, P.; Huang, Y. H. *ACS Nano* **2014**, *8*, 9295−9303.
(15) He, G.; Evers, S.; Liang, X.; Cuisinier, M.; Garsuch, A.; Nazar, L. F. *ACS Nano* **2013**, *7*, 10920−10930.
(16) Zhang, C. F.; Wu, H. B.; Yuan, C. Z.; Guo, Z. P.; Lou, X. W. *Angew. Chem.* **2012**, *124*, 9730−9733.
(17) Lu, S. T.; Cheng, Y. W.; Wu, X. H.; Liu, J. *Nano Lett.* **2013**, *13*, 2485−2489.
(18) Zheng, G. Y.; Zhang, Q.; Cha, J. J.; Yang, Y.; Li, W. Y.; Seh, Z. W.; Cui, Y. *Nano Lett.* **2013**, *13*, 1265−1270.
(19) Sun, L.; Li, M. Y.; Jiang, Y.; Kong, W. B.; Jiang, K. L.; Wang, J. P.; Fan, S. S. *Nano Lett.* **2014**, *14*, 4044−4049.
(20) Zhou, G. M.; Pei, S. F.; Li, L.; Wang, D. W.; Wang, S. G.; Huang, K.; Yin, L. C.; Li, F.; Cheng, H. M. *Adv. Mater.* **2014**, *26*, 625−631.
(21) Schuster, J.; He, G.; Mandlmeier, B.; Yim, T.; Lee, K. T.; Bein, T.; Nazar, L. F. *Angew. Chem.* **2012**, *124*, 3651−3655.
(22) Strubel, P.; Thieme, S.; Biemelt, T.; Helmer, A.; Oschatz, M.; Brückner, J.; Althues, H.; Kaskel, S. *Adv. Funct. Mater.* **2012**, *25*, 287−297.
(23) Zheng, G. Y.; Zhang, Q. F.; Cha, J. J.; Yang, Y.; Li, W. Y.; Seh, Z. W.; Cui, Y. *Nano Lett.* **2013**, *13*, 1265−1270.
(24) Tang, C.; Li, B. Q.; Zhang, Q.; Zhu, L.; Wang, H. F.; Shi, J. L.; Wei, F. *Adv. Funct. Mater.* **2016**, *26*, 577−585.
(25) Yoo, J.; Cho, S.-J.; Jung, G. Y.; Kim, S. H.; Choi, K.-H.; Kim, J.-H.; Lee, C. K.; Kwak, S. K.; Lee, S.-Y. *Nano Lett.* **2016**, *16*, 3292−3300.
(26) Naguib, M.; Comec, J.; Dyatkina, B.; Pressera, V.; Tabernac, P.-L.; Simonc, P.; Barsouma, M. W.; Gogotsi, Y. *Nat. Commun.* **2015**, *6*, 7760.
(27) Wang, Z. Y.; Dong, Y. F.; Li, H. J.; Zhao, Z. B.; Wu, H. B.; Hao, C.; Liu, S. H.; Qiu, J. S.; Lou, X. W. *Nat. Commun.* **2014**, *5*, 5002.

DOI: 10.1021/acs.nanolett.6b04433
Nano Lett. 2017, 17, 437−444

(28) Song, J. X.; Gordin, M. L.; Xu, T.; Chen, S. R.; Yu, Z. X.; Sohn, H.; Lu, J.; Ren, Y.; Duan, Y. H.; Wang, D. H. *Angew. Chem., Int. Ed.* **2015**, *54*, 4325−4329.
(29) Li, Z. Q.; Li, C. X.; Ge, X. L.; Ma, J. Y.; Zhang, Z. W.; Li, Q.; Wang, C. X.; Yin, L. W. *Nano Energy* **2016**, *23*, 15−26.
(30) Li, Y. J.; Fan, J. M.; Zheng, M. S.; Dong, Q. F. *Energy Environ. Sci.* **2016**, *9*, 1998−2004.
(31) Aijaz, A.; Masa, J.; Rösler, C.; Xia, W.; Weide, P.; Botz, A. J. R.; Fischer, R. A.; Schuhmann, W.; Muhler, M. *Angew. Chem., Int. Ed.* **2016**, *55*, 4087−4091.
(32) Wu, R. B.; Qian, X. K.; Zhou, K.; Wei, J.; Lou, J.; Ajayan, P. M. *ACS Nano* **2014**, *8*, 6297−6303.
(33) Jiang, J.; Zhu, J. H.; Ai, W.; Wang, X. L.; Wang, Y. L.; Zou, C. J.; Huang, W.; Yu, T. *Nat. Commun.* **2015**, *6*, 8622.
(34) Xia, B. Y.; Yan, Y.; Li, N.; Wu, H. B.; Lou, X. W.; Wang, X. *Nat. Energy* **2016**, *1*, 15006.
(35) Rehman, S.; Gu, X. X.; Khan, K.; Mahmood, N.; Yang, W. L.; Huang, X. X.; Guo, S. J.; Hou, Y. L. *Adv. Energy Mater.* **2016**, *6*, 1502518.
(36) Xiang, Z. H.; Xue, Y. H.; Cao, D. P.; Huang, L.; Chen, J. F.; Dai, L. M. *Angew. Chem., Int. Ed.* **2014**, *53*, 2433−2437.
(37) Paraknowitsch, J. P.; Thomas, A. *Energy Environ. Sci.* **2013**, *6*, 2839−2855.
(38) Tang, C.; Zhang, Q.; Zhao, M. Q.; Huang, J. Q.; Cheng, X. B.; Tian, G. L.; Peng, H. J.; Wei, F. *Adv. Mater.* **2014**, *26*, 6100−6105.
(39) Xiao, Z. B.; Yang, Z.; Wang, L.; Nie, H. G.; Zhong, M. E.; Lai, Q. Q.; Xu, X. J.; Zhang, L. J.; Huang, S. M. *Adv. Mater.* **2015**, *7*, 2891−2898.
(40) Zhou, G. M.; Zhao, Y. B.; Manthiram, A. *Adv. Energy Mater.* **2015**, *5*, 1402263.

DOI: 10.1021/acs.nanolett.6b04433
Nano Lett. 2017, 17, 437−444